Geochimica et Cosmochimica Acta, Vol. 69, No. 6, pp. 1543–1553, 2005

0016-7037/05 $30.00 + .00

doi:10.1016/j.gca.2004.08.032

A high-resolution TEM-AEM, pH titration, and modeling study of Zn^{2+} coprecipitation with ferrihydrite

STACIN MARTIN,[2,†] CHEN ZHU,[1,*] JOSEPH RULE,[2] NOEL T. NUHFER,[3] ROBERT FORD,[4] SHEILA HEDGES,[5] and YEE SOONG[5]

[1]Department of Geological Sciences, Indiana University, Bloomington, Indiana 47405-1405 USA
[2]Department of Ocean, Earth, and Atmospheric Sciences, Old Dominion University, Norfolk, Virginia 23529 USA
[3]Carnegie Mellon University, Department of Materials Sciences and Engineering, Pittsburgh, Pennsylvania 15260 USA
[4]Robert S. Kerr Environmental Research Laboratory, U.S. Environmental Protection Agency, Ada, Oklahoma 74820 USA
[5]National Energy Technology Laboratory, U.S. Department of Energy, Pittsburgh, Pennsylvania 15236 USA

(*Received September* 26, 2003; *accepted in revised form August* 30, 2004)

Abstract—Experiments of Zn^{2+} and Fe^{3+} coprecipitation as a function of pH were conducted in the laboratory at ambient temperature and pressure. X-ray diffraction patterns of the coprecipitates show two broad peaks at 0.149 and 0.258 nm, which is consistent with published patterns for pure 2-line ferrihydrite. Zn^{2+} uptake occurred at pH ≥5 while Fe^{3+} precipitation occurred between pH 3 and 4, although both Zn^{2+} and Fe^{3+} were present in the same solution during the entire range of pH titration. High-resolution transmission electron microscopy shows that the coprecipitates are 2 to 6 nm sized single crystalline particles but aggregated to 50 to 400 nm sized clusters. Analytical electron microscopy indicated that the 5% atomic Zn with respect to Fe was homogeneously distributed. No segregated phases were found in the clusters or at single crystal edges, which is consistent with published extended X-ray absorption fine structure (EXAFS) results at similar Zn/(Zn + Fe) ratios. Hence, occlusion and surface precipitation may be excluded as possible coprecipitation mechanisms. The bulk solution Zn^{2+} sorption edge was fitted to both solid solution and generalized diffuse layer surface complexation models. However, a solid solution model is inconsistent with published EXAFS results that show tetrahedral polydentate Zn^{2+} complexes sharing apices with Fe^{3+}octahedra. *Copyright © 2005 Elsevier Ltd*

1. INTRODUCTION

The mobility, transport, distribution, and cycling of trace elements in subsurface and surface geological systems have long been of interest to geochemists. Iron oxyhydroxides occur widely in surficial and subsurface geological environments and likely play a prominent role in regulating trace element geochemistry. Even though iron oxyhydroxides may constitute a minor fraction of the bulk rock, soil, or sediment, they are efficient scavengers of metals and radionuclides and may dominate the adsorptive properties of the solid matrix (Krauskopf, 1956; Jenne, 1968; Davis and Kent, 1990). However, the mechanisms by which trace elements are sorbed onto iron oxyhydroxides in pristine and anthropogenically impacted natural water-rock systems are largely unknown. The knowledge of sorption mechanisms is nevertheless central to developing quantitative partitioning models that serve as a theoretical basis for the use of trace elements as signatures of fluid flow, chemical reactions, and other geological and environmental processes, and for the prediction of contaminant transport in geological media.

Coprecipitation (CPT) is commonly referred to as the simultaneous removal of a trace constituent together with a carrier constituent from a homogeneous aqueous solution. Laboratory experiments show that Al^{3+} (Schulze and Schwertmann, 1984; Wolska and Schwertmann, 1993); Cr^{3+} (Schwertmann et al., 1989; Manceau et al., 1992); Mn^{2+}, Ni^{2+}, and Co^{2+} (Stiers and Schwertmann, 1985; Schwertmann and Cornell, 1991); and Cu^{2+}, Zn^{2+}, and Cd^{2+} (Gerth, 1990) can substitute for Fe^{3+} in goethite. Cr^{3+} and Fe^{3+} coprecipitate to form an amorphous solid solution (Sass and Rai, 1987; Amonette and Rai, 1990), and Zn^{2+}, Pb^{2+}, Ni^{2+}, Cu^{2+}, UO^{2+} coprecipitate with amorphous iron hydroxides (Crawford et al., 1993; Bruno et al., 1995; Martinez and McBride, 1998; Karthikeyan et al., 1999; Duff et al., 2002). Natural goethites often contain trace amounts of foreign cations (Gerth, 1990; Manceau et al., 2000).

Despite its importance, the mechanism of coprecipitation is poorly understood. The term *coprecipitation* is loosely used in a phenomenological sense, alluding to the century-old observations that trace constituents, often metals, are removed together with a major constituent from a homogeneous aqueous solution. The mechanisms may be surface adsorption, surface precipitation, incorporation of the tracer into the carrier structure forming a solid solution, mechanical envelopment by the carrier, or a combination of all the above. In the following discussion, "coprecipitation experiments" are referred to designs in which the tracer (e.g., Zn^{2+}) is present when the carrier ion (e.g., Fe^{3+}) precipitates to form hydrous oxides (Fig. 1). In "adsorption experiments (ADS)," the tracer is added to a suspension of already precipitated hydrous oxides of the carrier ion. The term "sorption" refers to all processes that transfer an ion from the aqueous to the solid phase (Sposito, 1984; Koretsky, 2000), without reference to the types of processes (e.g., CPT or ADS).

Previous work shows that sorption isotherms and sorption pH edges prepared with ADS and CPT experimental procedures are appreciably different for Cu^{2+} sorption onto hydrous iron and aluminum oxides (Karthikeyan et al., 1997;

* Author to whom correspondence should be addressed (chenzhu@indiana.edu).
† *Present address:* CH2M HILL, Inc., 5700 Thurston Ave., Suite 120, Virginia Beach, Virginia 23455 USA.

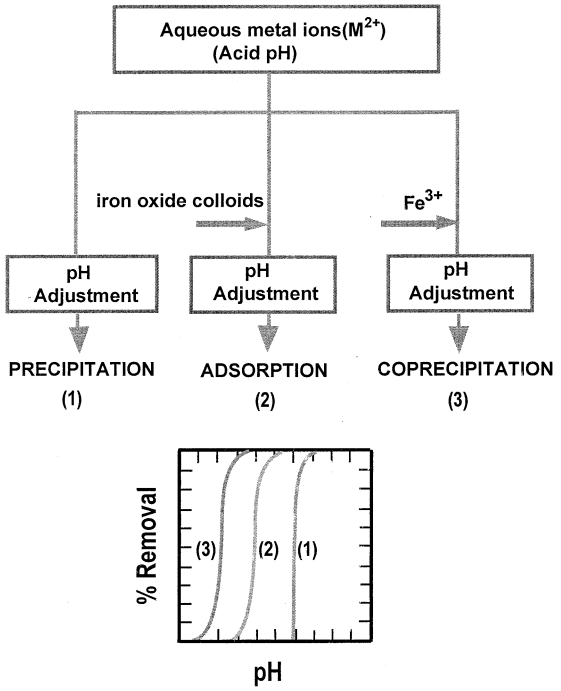

Fig. 1. Schematic representation of the coprecipitation experiments in comparison to adsorption and solubility experiments. Modified from Crawford et al. (1993).

Karthikeyan et al., 1999), As(V) sorption onto ferrihydrite (Fuller et al., 1993), and Ni^{2+} and Cr^{3+} sorption onto hydrous iron oxides (Crawford et al., 1993), with coprecipitation as the more efficient process for metal removal from aqueous solutions. There is also great interest concerning whether metals removed by the CPT processes are more permanently immobilized than those by the ADS process. Fuller et al. (1993) argued that coprecipitation experiments more resemble contamination in many field situations than ADS experimental conditions, under which the iron oxyhydroxide particles are aged for a few hours to a few days before metal adsorbates are brought into contact with them. For example, in acid mine drainage intrusion into groundwater, low-pH mine water can react with calcite in the aquifer. Ferric iron and a suite of trace toxic metals and radionuclides precipitate simultaneously in response to the rise of pH (Zhu et al., 2002). However, most of the previous work on metal and iron oxyhydroxide interactions focus on surface adsorption (see review by Dzombak and Morel, 1990). There are only a few coprecipitation studies, but these studies either produced only bulk chemistry data (Crawford et al., 1993; Karthikeyan et al., 1997), which cannot be used to discern the microscopic mechanisms (Sposito, 1986), or obtained spectroscopic data on samples synthesized at a particular pH (Duff et al., 2002; Waychunas et al., 2002; Waychunas et al., 2003), which makes it difficult to extrapolate the molecular level results to macroscopic models.

This paper presents a solution chemistry, high-resolution electron microscopy, and modeling study of coprecipitation of Zn^{2+} with ferric iron. There is a large literature base on adsorption of Zn^{2+} onto hydrous ferric oxides (see review by Dzombak and Morel, 1990), but studies of coprecipitation of Zn^{2+} with hydrous ferric oxides are limited (Crawford et al., 1993; Martinez and McBride, 1998). Waychunas et al. (2002, 2003) conducted comprehensive extended X-ray absorption fine structure (EXAFS) studies on precipitates from both CPT and ADS experiments at pH 6.5, and many earlier works are referred to and discussed in Waychunas et al. (2002).

2. EXPERIMENTAL METHODS

In all instances, the batch experiments were conducted at room temperature (22°C) and in the presence of ambient CO_2. All reagents, acquired from Fisher Scientific, were of analytical grade unless otherwise indicated. An Fe-Zn solution containing 7.8 mM $(Fe(NO_3)_3$ and 0.57 mM Zn was made from ferric nitrate $(Fe[NO_3]_3 \cdot 9H_2O$, purity 99.1%) and zinc nitrate. All solutions were prepared in 10 mM KNO_3 background electrolyte solution. A 100-mL aliquot of the Fe-Zn solution was transferred to a 250-mL polypropylene bottle. The pH of the solution was measured before the titration using a Beckman Φ34 pH meter and Orion combination electrode with a replaceable junction calibrated with three buffers (pH = 2, 7, and 10). While stirring the solution vigorously, 0.5-mL volumes of 0.1 M KOH were added cumulatively to successive bottles containing the Fe-Zn^{2+} solution using a burette at a rate of 6-mL min^{-1}. After the samples were titrated, they were left to equilibrate at 22°C for 24 or 30 h, at which time the pH was measured. Measurements at every hour up to 100 h confirmed that solution pH had stabilized after 24 h.

The solids were separated by centrifugation at a rate of 3910 RCF for 45 min, and the supernatant liquid decanted. All supernatants were either vacuum filtered using 0.2 μm membrane filters or filtered using a cellulose membrane filter connected to a 30-mL of polypropylene syringe. The filtered supernatants were clear. The pH of the supernatant liquid was then measured again, and the solution was then acidified using concentrated HCl. Then 50 mL of each supernatant liquid was concentrated by evaporation to 25 mL. These solutions were analyzed for Fe and Zn using a Perkin Elmer 5000 Flame AAS. To minimize matrix interference, calibration standards were precisely matched with samples in terms of matrix. The detection limit for Fe and Zn was ~0.1 mg L^{-1} or 10^{-6} M. The solids were washed to remove electrolytes with 50 mL of DI H_2O by shaking for 5 min and then centrifuged at a rate of 3190 RCF for 45 min to separate the solids and the wash. Precipitates from one set of titration experiments were freeze-dried for preservation, and from another set left on moist filter papers that were subsequently stored in capped vials. All supernatants were stored at 4°C until analysis.

The solid specimens were prepared for examination by high-resolution transmission electron microscopy (HRTEM). The freeze-dried precipitates were examined two months following the titration experiments, and the precipitates retained on filter papers examined one yr of titration experiments. The coprecipitates were ultrasonicated in ethanol alcohol to resuspend the particles. The suspension of coprecipitates was pipetted onto a holey-carbon support film supported by a copper-mesh TEM grid and air-dried. The suspension of coprecipitates in ethanol was cooled during the ultrasonic process to prevent any possible formation of crystalline iron minerals.

The specimens from coprecipitation at pH 6 were observed with a Philips FEI Tecnai F20 TEM/STEM with point-to-point resolution of 0.24 nm, a Gatan Imaging Filter and Energy Dispersive X-ray (EDX), and a Jeol 4000EX with point-to-point resolution of 0.17 nm, with a Gatan Imaging Filter. The Philips FEI Tecani F20 TEM/STEM was used for high-resolution imaging and for microanalysis. The Jeol 4000EX HRTEM was used to obtain the highest possible lattice imaging resolution.

Powder X-ray diffraction of the coprecipitates was performed on a Philips X'pert Diffractometer and a Rigaku Miniflex Diffractometer with Fe Kα radiation (30 kV, 15 mA). Samples were prepared by grinding them gently and were mounted as smears on a zero-background quartz plate using ethanol. For reference, a 2-line ferrihydrite synthesized by the method of Schwertmann and Cornell (1991) was also analyzed. The synthetic 2-line ferrihydrite reference was mounted as a pressed powder in the cavity of a quartz plate. The scans used a 0.01° step size, and ranged from 10 to 100°.

Table 1. Coprecipitation experimental data.

Set 1		Set 2	
pH	Zn^{2+} (mM)	pH	Zn^{2+} (mM)
2.28	0.569	2.45	0.592
2.24	0.454	2.78	0.573
2.35	0.746	3.26	0.569
2.44	0.725	3.40	0.580
2.52	0.623	3.81	0.583
2.62	0.496	4.04	0.538
2.89	0.45	4.82	0.528
3.00	0.458	4.92	0.452
3.22	0.499	5.84	0.263
3.54	0.542	5.93	0.174
3.88	0.514	6.26	0.0826
4.07	0.464	7.22	0.00517
4.44	0.482	7.84	0.00152
4.21	0.528	9.51	0.00451
4.61	0.459	10.66	0.00201
4.55	0.470		
4.81	0.559		
4.9	0.476		
4.39	0.438		
4.46	0.465		
4.73	0.454		
5.16	0.449		
5.14	0.422		
5.39	0.39		
5.81	0.213		
5.80	0.153		
5.99	0.048		

3. RESULTS

3.1. Bulk Solution Chemistry Data

The solution chemical data from the pH titration experiments are listed in Table 1 and shown in Figure 2. Zn^{2+} uptake from the solution during pH titration mostly occurred at pH $\geq$5. At about pH 6.3, nearly all of the Zn^{2+} in the solution was sorbed onto solids (Fig. 2a). We also analyzed Fe^{3+} concentrations during the pH titration. Although the Fe data are somewhat scattered, it is clear that most Fe^{3+} precipitated between pH 3 and 4 (Fig. 2b). Thus, mechanical enveloping, as suggested by previous studies (Schroth, 1994), does not appear to be the dominant mechanism in our experiments.

3.2. X-ray Diffraction Data

Two broad peaks at a *d*-spacing of 0.149 and 0.258 nm, respectively, were observed (Fig. 3a). This X-ray diffraction (XRD) pattern is consistent with the reference of pure 2-line ferrihydrite (Fig. 3b), synthesized according to the method of Schwertmann and Cornell (1991), and consistent with published patterns of synthetic and natural 2-line ferrihydrite (Cornell and Schwertmann, 1996). Janney et al. (2000b) reviewed earlier XRD and TEM work on 2-line ferrihydrite, as well as the naming conventions. We follow their choice and refer to our coprecipitate as "2-line ferrihydrite (2LFh)" even though our precipitate contains zinc, but also use it interchangeably with "hydrous ferric oxide (HFO)" after Dzombak and Morel (1990).

3.3. High-Resolution Transmission and Analytical Electron Microscopy Observations

High-resolution microscopy shows that the Zn-Fe coprecipitates are spherical crystalline particles, sized from 2 to 6 nm, with an average of ~5 nm in diameter (Fig. 4). The particles form clusters from 50 nm to 400 nm in size. Each particle is a single nanocrystal. Within each particle, lattice images show a single orientation. These features of these Zn-Fe coprecipitates are similar to those observed by Janney et al. (2000a) for pure 2-line ferrihydrite, which indicates that incorporation of up to 5% zinc into 2-line ferrihydrite does not alter the morphology of the particles. Previous TEM studies of 2-line ferrihydrite are reviewed by Janney et al. (2000a).

No apparent differences were observed between samples freeze-dried and those retained on filter papers, other than appearing to be more crystalline in the samples retained on filter papers (Fig. 4a and b). More extensive electron microscopic work was conducted on the precipitates on filter papers. Cornell and Schwertmann (1996) show that sorbed metals can significantly retard ferrihydrite transformations.

No additional phases (segregated Zn phases, e.g., ZnO, $Zn(OH)_2$, $ZnCO_3$) were found. From this observation, we conclude that occlusion is not a major mechanism of coprecipitation in our experiments. Aging or recrystallization of ferrihydrite tends to segregate coprecipitated foreign ions (Waychunas et al., 1993; Cornell and Schwertmann, 1996). The fact that no segregated occlusion was found in samples aged from two months to a year obviates its existence at earlier times. Previous experiments and theoretical modeling suggested that, at high-surface coverage (e.g., >10%), the sorbate may form a surface precipitate that is comprised of the sorbate and sorbent ion to form a solid solution, despite sorbate concentrations that are below the saturation of suspected precipitate $Zn(OH)_{2(c)}$ (Farley et al., 1985). In our experiments, the Fe:Zn mole ratio is 1:0.068. When all the zinc is sorbed, ~37% surface sites are covered with Zn^{2+}, according to the surface site densities recommended by Dzombak and Morel (1990). Based on EXAFS and X-ray absorption near-edge spectroscopy (XANES), Waychunas et al. (2002, 2003) suggested the formation of a Zn-containing precipitate with a brucite layer topology on Fe-Zn coprecipitate surfaces at a much higher surface coverage than for our samples (0.5 vs. 0.05 Zn/(Zn+Fe). Karthikeyan et al. (1999) report surface precipitates as the dominant mechanism at high-sorbate/sorbent ratios for Cu^{2+} coprecipitation with hydrous aluminum oxides. Trainor et al. (2000) found the formation of a hydrotalcite precipitate on alumina using the X-ray absorption spectrum (XAS) methods. Towle et al. (1997) found $Co(OH)_2$ type surface precipitate formed on Al_2O_3 surfaces. However, in our samples, lattice images with point-to-point resolution of 0.17 nm do not show phases of different structures at the edges of the particles (Fig. 5). This is consistent with EXAFS work on coprecipitates with a similar Zn/Zn+Fe ratio to our samples (Waychunas et al., 2002). No massive defects were observed in the crystallites either, which also agrees with previous spectroscopic work that shows limited incorporation of Zn^{2+} into the ferrihydrite structure (Waychunas et al., 2002, 2003).

The results from our STEM/EDX analysis show that the clusters contain Fe, O, and Zn, with an average of Zn being ~5

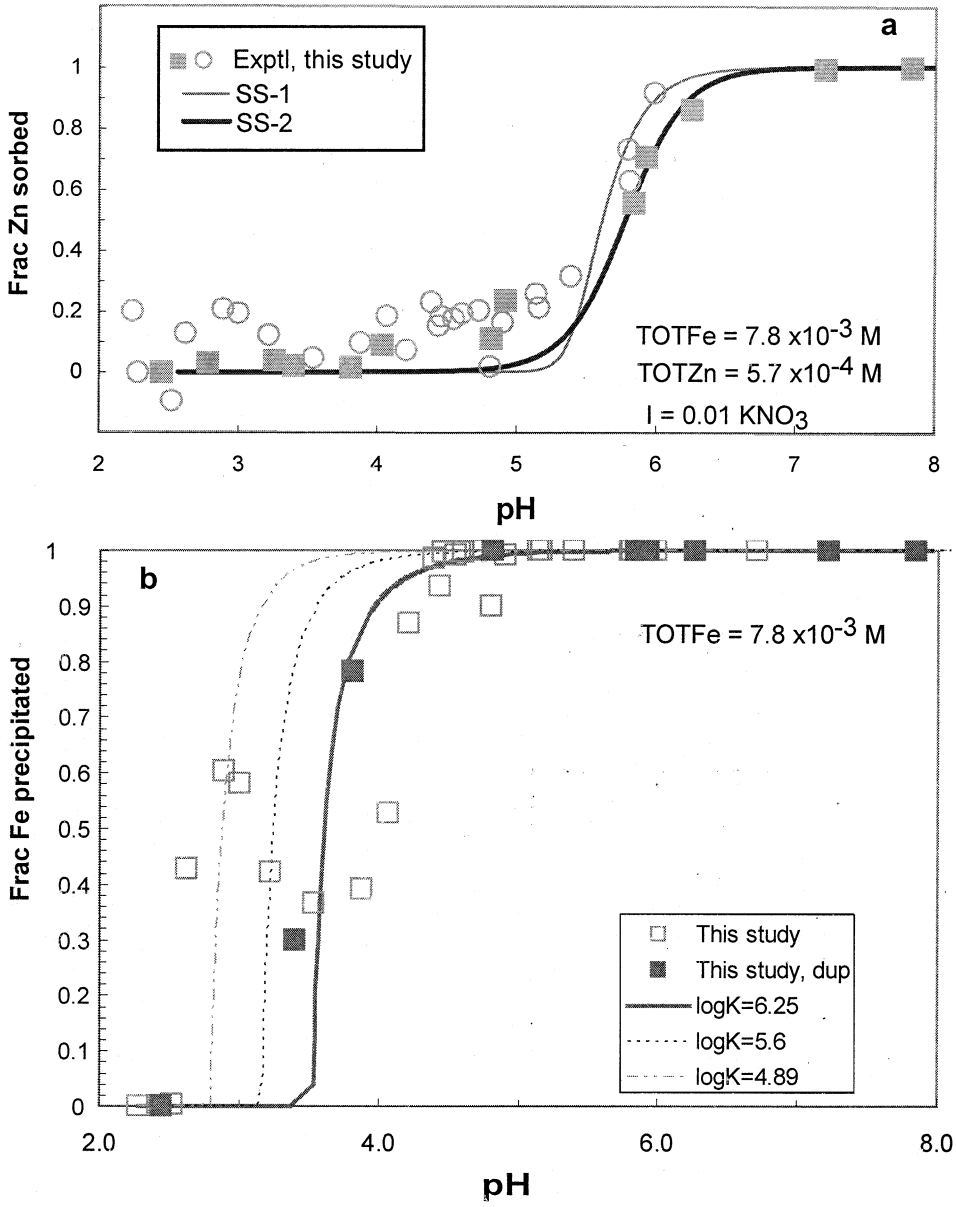

Fig. 2. Zn^{2+}-Fe^{3+} coprecipitation. (a) Symbols are Zn^{2+} experimental data and lines are modeling results. Circles and squares represent duplicate experiments. SS-1 stands for $(Fe_2, Zn_3)(OH)_6$ and SS-2 for $(Fe, ZnH)(OH)_3$ solid solution models discussed in the text; (b) Fe^{3+} concentrations as a function of titrated pH. Lines are solubility calculations (with speciation) with equilibrium constants from Wagman et al. (1982; 5.6), Nordstrom et al. (1990; 4.89), and the best fit (6.25).

atomic %. This Zn concentration agrees with the mole balance of 4.8 atomic % at pH 6 derived from solution chemistry. The EDX results were based on over forty EDX spectra and showed no Zn-concentrated areas, indicating that the Zn is homogeneously distributed. The probe size for the analysis was 0.5 nm at 1 nA of beam current, but the specimen preparation did not completely desegregate the individual grains, and therefore, most analyses sampled overlapped particles. The results derived from electron energy loss imaging with a Gatan imaging filter have also shown no particles containing high concentration of Zn. It is beyond the resolution limit to distinguish whether Zn^{2+} is concentrated on the edges/surfaces of, or evenly distributed within, the individual particles.

3.4. Thermodynamic Modeling

The pH titration data presented in Figure 2 allow us to simulate Zn^{2+} sorption with both solid solution and surface complexation models. The geochemical modeling code PHREEQC (Parkhurst and Appello, 1999) was used for the simulation. The standard states for the solids are defined as unit activity for pure solids at the temperature and pressure of interest. The standard state for water is the unit activity of pure water. For aqueous species other than H_2O, the standard state is the unit activity of the species in a hypothetical one molal ideal solution referenced to infinite dilution at the temperature and pressure of interest. Standard states for the surface sites are the

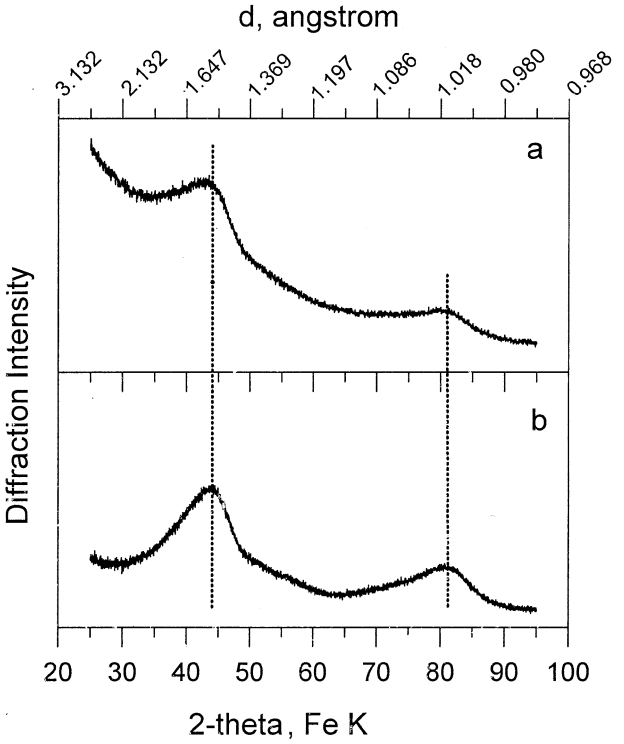

Fig. 3. X-ray diffraction data showing characteristic pattern for 2-line ferrihydrite: (a) Fe-Zn coprecipitate; and (b) 2-line ferrihydrite synthesized by method of Schwertmann and Cornell (1991).

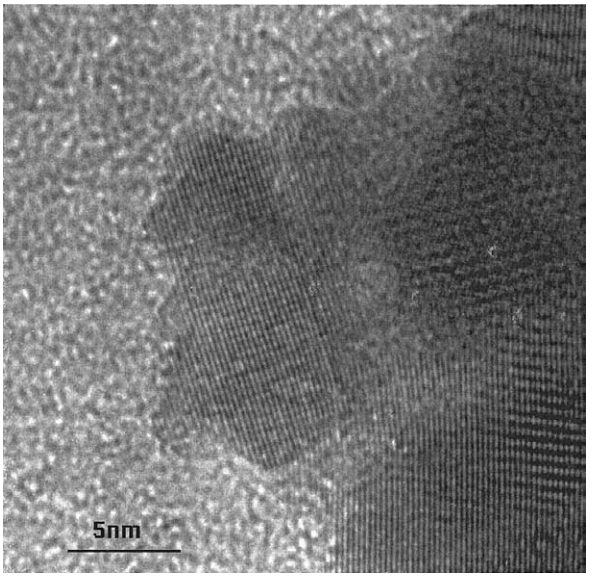

Fig. 5. HRTEM image of Fe^{3+} and Zn^{2+} coprecipitates, showing lattice images of single crystallites. The lines are individual atomic planes. The right-hand side of the center image shows overlapping particles with lattice planes at different orientations and producing an interface fringe.

unit activity of a completely unsaturated surface at pressure and temperature of interest, and for surface species, the unit activity on a completely saturated surface with zero potential with reference to infinite dilution at P, T of interest (Sverjensky, 2003). The thermodynamic properties used in the simulations are listed in Table 2.

3.4.1. Solid solution models

For solid solution formation, two different models were evaluated to account for the stoichiometry of solid solutions of ions with different valences. The first (SS-1) takes the

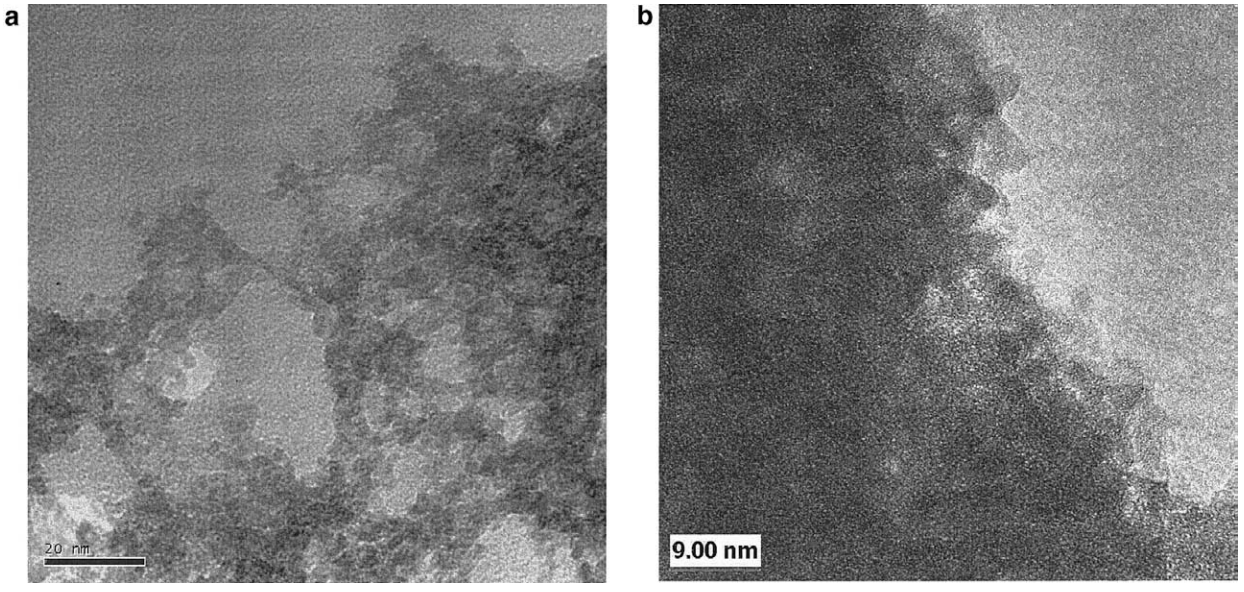

Fig. 4. TEM image of Fe^{3+} and Zn^{2+} coprecipitates on holey carbon support. (a) precipitates retained on filter paper and examined one yr after titration experiments; and (b) precipitates freeze-dried and examined two months after titration experiments.

Table 2. Equilibrium constants used in modeling.

Species	Reactions	log *K*	Ref
	Aqueous species		
$FeOH^{++}$	$Fe^{3+} + H_2O = FeOH^{2+} + H^+$	−2.19	a
$Fe(OH)_2^+$	$Fe^{3+} + 2H_2O = Fe(OH)_2^+ + 2H^+$	−5.67	a
$Fe(OH)_3^\circ$	$Fe^{3+} + 3H_2O = Fe(OH)_3^\circ + 3H^+$	−12.56	a
$Fe(OH)_4^-$	$Fe^{3+} + 4H_2O = Fe(OH)_4^- + 4H^+$	−21.6	a
$Fe_3(OH)_4^{5+}$	$3Fe^{3+} + 4H_2O = Fe_3(OH)_4^{5+} + 4H^+$	−6.3	a
$Fe_2(OH)_2^{4+}$	$2Fe^{3+} + 2H_2O = Fe_2(OH)_2^{4+} + 2H^+$	−2.95	a
$ZnOH^+$	$Zn^{2+} + H_2O = ZnOH^+ + H^+$	−8.96	d
$Zn(OH)_2^\circ$	$Zn^{2+} + 2\ H_2O = Zn(OH)_2^\circ + 2\ H^+$	−16.9	d
$Zn(OH)_3^-$	$Zn^{2+} + 3\ H_2O = Zn(OH)_3^- + 3\ H^+$	−28.4	d
$Zn(OH)_4^{2-}$	$Zn^{2+} + 4\ H_2O = Zn(OH)_4^{2-} + 4\ H^+$	−41.2	d
	Surface species		
$Hfo\_wOH_2^+$	$Hfo\_wOH + H^+ = Hfo\_wOH_2^+$	7.29	b
Hfo_wO^-	$Hfo\_wOH = Hfo\_wO^- + H^+$	−8.93	b
Hfo_sOZn^+	$Hfo\_sOH + Zn^{2+} = Hfo\_sOZn^+ + H^+$	0.99	b
Hfo_wOZn^+	$Hfo\_wOH + Zn^{2+} = Hfo\_wOZn^+ + H^+$	−1.99	b
	Solid species		
$Zn(OH)_{2\ (c)}$	$Zn(OH)_2 + 2H^+ = Zn^{2+} + 2H_2O$	11.50	d
$Fe(OH)_{3(am)}$	$Fe(OH)_3(a) + 3H^+ = Fe^{3+} + 3H_2O$	5.6	c
§$ZnH(OH)_{3(s)}$	$ZnH(OH)_2 + 2H^+ = Zn^{2+} + 3H_2O$	9.1	e
§$Zn(OH)_{2(s)}$	$Zn(OH)_2 + 2H^+ = Zn^{2+} + 2H_2O$	7.83	e

a: Nordstrom et al. (1990); b: Dzombak and Morel (1990); c: Wagman et al. (1982); d: Ball and Nordstrom (1991); e: retrieved from experimental data in this study.
§ Solid solution components.

three-for-two substitution to compensate for the charge imbalance,

$$Fe_2(OH)_{6(s)} + 6H^+ = 2Fe^{3+} + 6H_2O \quad (1)$$

$$Zn_3(OH)_{6(s)} + 6H^+ = 3Zn^{2+} + 6H_2O \quad (2)$$

Here, $Fe_2(OH)_{6(s)}$ and $Zn_3(OH)_{6(s)}$ stand for the end members of the solid solution. In doing so, we assume that the precipitated iron oxyhydroxide has a nominal formula of $Fe(OH)_{3(am)}$ (Dzombak and Morel, 1990). Coprecipitation was modeled as an ideal solid solution. This is appropriate for solid solutions in which the trace metal component has a small mole fraction in the solid solution. If Henrian standard states are defined as hypothetical pure $M_3(OH)_6$ end members of the solid solution with an $Fe(OH)_{3(am)}$ structure, extrapolated from the infinitely dilute solution regions where Henry's law is obeyed, and a Raoultian standard state remains for the $Fe_2(OH)_6$ end member, the activity coefficients for both $Fe_2(OH)_6$ and trace end members are unity in the dilute solution regions where Henry's law is obeyed for the tracer (Ganguly and Saxena, 1987). By trial and error, a log *K* of 23.4 for reaction (2) was found to best fit the experimental data, which, as expected, is much smaller than the solubility products for pure $Zn(OH)_{2(c)}$ solid (when the stoichiometry for reaction (2) is written as the same). As mentioned above, the former is a hypothetical end-member component of the solid solution that holds the $Fe(OH)_{3(am)}$ structure. This model produces a sorption edge that is overly steep when compared to experimental data (Fig. 2).

A second solid solution model (SS-2) takes the stoichiometry of

$$Fe(OH)_{3(s)} + 3H^+ = Fe^{3+} + 3H_2O \quad (3)$$

$$ZnH(OH)_{3(s)} + 2H^+ = Zn^{2+} + 3H_2O \quad (4)$$

Here, we assume that the one-for-one substitution of Zn^{2+} for Fe^{3+} is compensated by an addition of H^+ into the crystalline structure or a replacement of OH^- for O^{2-} (e.g., Waychunas et al., 2002). Again, when a Henrian standard state is defined as hypothetical pure $ZnH(OH)_{3(s)}$ end members of the solid solution with an $Fe(OH)_{3(am)}$ structure, extrapolated from the infinitely dilute solution regions where Henry's law is obeyed, and a Raoultian standard state remains for the $Fe(OH)_3$ end member, the activity coefficients for both Fe $(OH)_3$ and $ZnH(OH)_{3(s)}$ are unity in the dilute solution regions where Henry's law is obeyed for the tracer (Ganguly and Saxena, 1987). A best fit to the experimental data resulted from a log *K* of 9.1 for reaction (4). Figure 2 demonstrates that SS-2 fits the experimental sorption edges better than SS-1. Variations of the log *K* for the HFO solubility reaction, $Fe(OH)_{3(am)} + 3H^+ = Fe^{3+} + 3H_2O$, did not reveal notable differences in either of the solid solution models.

3.4.2. *Surface complexation models*

The generalized diffuse layer model (Dzombak and Morel, 1990) was used for modeling surface adsorption. Other electrostatic surface adsorption models have been proposed, e.g., constant capacitance and triple layer models, but all electrostatic models can describe limited experimental sorption data sets (Westall and Hohl, 1980; Venema et al., 1996). Dzombak

Table 3. Best-fit surface properties and adsorption constants for Zn-Fe coprecipitation experiments.

Properties		Values
Site density (N_s)		
weak (w)		0.8 mol/mol[†]
strong (s)		0.02 mol/mol[†]
Surface area		600 m^2/g
Formula weight		89 g/mol
Surface species		**log *K***
$Hfo\_wOH_2^+$	$Hfo\_wOH + H^+ = Hfo\_wOH_2^+$	7.89[†]
Hfo_wO^-	$Hfo\_wOH = Hfo\_wO^- + H^+$	−8.33[†]
Hfo_sOZn^+	$Hfo\_sOH + Zn^{2+} = Hfo\_sOZn^+$	1.59[†]
Hfo_wOZn^+	$Hfo\_wOH + Zn^{2+} = Hfo\_wOZn^+$	−0.39[†]

[†] Best-fit in this study. Surface area and formula weight are from Dzombak and Morel (1990). s = strong site; w = weak site.

and Morel (1990) provided a consistent theory and self-consistent database of equilibrium constants for adsorption onto hydrous ferric oxides. In particular, Dzombak and Morel (1990) reviewed Zn^{2+} adsorption experimental data and developed a two-site model for Zn^{2+} adsorption, a "weak" site (Hfo_w) and a "strong" site (Hfo_s), through the reactions:

$$Hfo\_sOH + Zn^{2+} = Hfo\_sOZn^+ + H^+ \quad (5)$$

$$Hfo\_wOH + Zn^{2+} = Hfo\_wOZn^+ + H^+ \quad (6)$$

Intrinsic surface complexation constants for reactions (5) to (6) and Zn^{2+} hydrolysis constants are listed in Table 2. Other surface properties are listed in Table 3.

Recognizing the differences that may exist in metastable precipitates, e.g., earlier access to a large number of active surface sites in CPT experiments (Fuller et al., 1993; Karthikeyan and Elliott, 1999), surface properties have been varied in modeling to match experimental data. When the surface site density, N_s, and surface areas were varied, the surface complexation equilibrium constants were adjusted for the corresponding hypothetical 1.0 molar standard states that depend on surface properties (Sverjensky, 2003). However, modeling results are insensitive to the variation of surface areas when site densities have been calculated on a per mole sorbent basis. This conclusion is consistent with the findings of Crawford et al. (1993) and Karthikeyan and Elliott (1999). In our calculations, the specific surface areas were varied to 400, 600, 700, and 5000 m^2/g, and only the surface area of 5000 m^2/g resulted in a slightly better fit. Geometric surface areas of 5 nm-diameter spheres are 340 m^2/g when a particle density of 3.57 g/cm^3 is adopted (Dzombak and Morel, 1990).

Increase of weak site density from 0.2 mol/mol Fe to 0.4 and 0.8 mol/mol Fe displaces the sorption edges to a lower pH and increase the steepness of the sorption curves (Fig. 6a, b). In the model, the weak and strong site densities were allowed to increase proportionally (Dzombak and Morel, 1990), and all surface complexation equilibrium constants were adjusted for standard state effects (Sverjensky, 2003). However, even at a site density of 0.8 mol/mol Fe, the sorption edge is still located at too high a pH (Fig. 6b). A value of 0.8 mol/mol Fe corresponds to site density of about 9 sites/nm^2, with the specific surface area and formula weight values listed in Table 3. Although a wide range of site densities are found for hematite, Christl and Kretzschmar (1999) found surface site densities between 5 to 10 sites/nm^2 best predicts competitive sorption, which should have better constraints on site density (Dzombak and Morel, 1990). A larger intrinsic complexation constant would move adsorption edges to lower pH and remove M^{2+} to lower levels (Fig. 6e). Increasing complexation constants for the strong site has little effect because of their low site concentrations. Adjustments of site density to 0.8 mol/mol Fe and of log *K* for reaction (5) and (6) one order of magnitude higher than those from Dzombak and Morel (1990) resulted in a match with experimental data (Fig. 6f).

Crawford et al. (1993) conducted both surface adsorption (ADS) and coprecipitation (CPT) experiments for Zn^{2+} (Table 4). However, their Zn^{2+} concentrations at the same pH are higher than those in our experiments and cannot be fitted to the surface complexation model that best fit our experimental data, even though the different Fe:Zn ratio and electrolyte background solutions in their experiments were all taken into account in the modeling. Their results for the two different experiments are also close to each other (Fig. 6c, d), a significant departure from other paired ADS-CPT datasets for Ni^{2+}, Cr^{3+} sorption onto hydrous ferric oxides (Crawford et al., 1993) and Cu^{2+} sorption onto hydrous ferric and aluminum oxides (Karthikeyan et al., 1999). Both sets of data from Crawford et al. (1993) can be modeled using the diffuse two-layer model (DLM) model with the parameters recommended by Dzombak and Morel (1990) by adjusting the weak site density from 0.2 to 0.4 mol/mol Fe (Fig. 6c and d). Crawford et al. (1993) measured solution chemistry after 40 min, whereas in our experiments, Fe and Zn were measured after 24 or 30 h. Dzombak and Morel (1990) point out the need of ~4 h for the solution chemistry to stabilize. EXAFS study of coprecipitates by Waychunas et al. (2002) shows the precipitation of a zinc hydroxide polymer at a Zn/(Zn+Fe) ratio of 0.127, smaller than the 0.15 ratio in the experiments of Crawford et al. (1993). The precipitates were not characterized in the study of Crawford et al. (1993).

4. DISCUSSION AND CONCLUDING REMARKS

Paired ADS-CPT experiments in metal/Fe-Al-Cr oxyhydroxide systems published in the literature show markedly different sorption behaviors, with the exception of Crawford et al.'s (1993) Zn^{2+} sorption onto ferrihydrite. pH sorption edges in CPT experiments are located at lower pH than those in the ADS experiments (Crawford et al., 1993; Karthikeyan et al., 1997; Karthikeyan and Elliott, 1999; Karthikeyan et al., 1999). In other words, at the same pH and sorbate/sorbent ratio, CPT removes metal ions more efficiently than ADS under otherwise identical experimental conditions. Furthermore, Karthikeyan et al. (1997) found 15% less Cu^{2+} was extracted by EDTA from ferrihydrite prepared by CPT procedure than those by ADS procedure under otherwise similar experimental conditions, and suggested that a part of

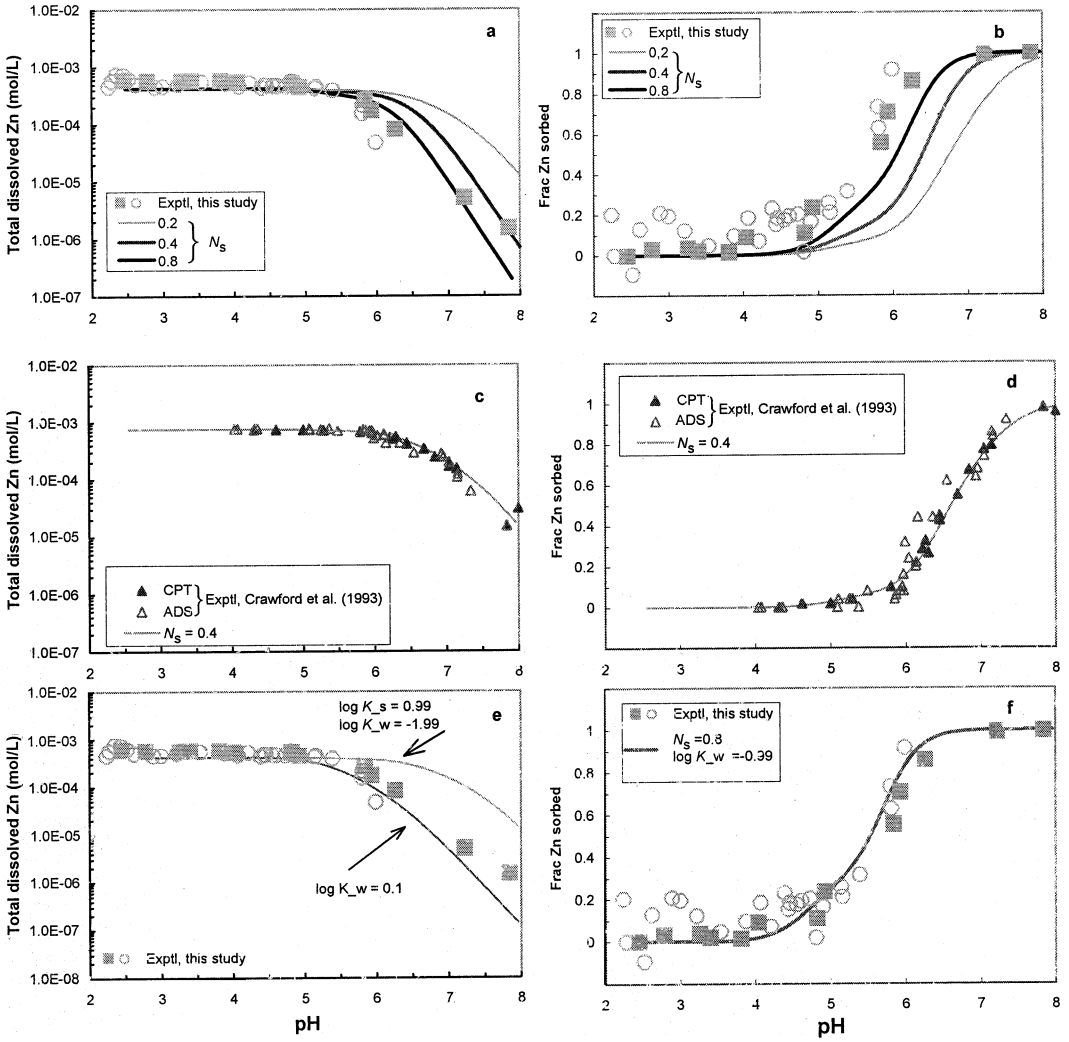

Fig. 6. Modeling surface complexation using the generalized diffuse layer model (DLM). Model parameters are listed in Tables 2 and 3 unless otherwise indicated in the graphs. (a) and (b): Comparison of experimental data to models with various site densities (N_s); (c) and (d): comparison of modeling results with the Crawford et al. (1993) experimental data. CPT and ADS represent coprecipitation and adsorption experiments, respectively. The line is from the DLM with N_s = 0.4 mol weak site /mol Fe and other surface properties and equilibrium constants listed in Tables 2 and 3, adjusted for this site density value; (e) comparison of experimental data to models with variation of intrinsic complexation constants; and (f) comparison of experimental data to models with best fit complexation constants and site density.

Cu^{2+} in the CPT experiments was incorporated into ferrihydrite structure or as segregated particle occlusion. This argument is important to environmental issues, regarding whether metal sorbed by the CPT procedure represents better long-term immobility and whether structural incorporation can explain the often observed hysteresis. Schultz et al. (1987) found that coprecipitated Zn^{2+} desorbed less than adsorbed Zn^{2+} at a lower pH.

Shaw et al. (2004) used time-resolved small angle X-ray scattering (SAXS) technique to study oxidative hydrolysis of

Table 4. Experimental conditions

	Fe^{3+} (mM)	Zn^{2+} (mM)	Fe:Zn total	Zn/(Zn + Fe) in precipitates	pH	Background solutions (mM)
This study	7.8	0.57	1:0.07	0.05†	6.0†	10 KNO_3
Waychunas et al. (2002)	1.0	0.01–1.0	1:0.01–1	0.009–1.0	6.5	100 $NaNO_3$
Crawford et al. (1993)	4.48	0.76	1:0.17			1.0 KNO_3

† Used for TEM study. All studies used $Fe(NO_3)_3$ and $Zn(NO_3)_2$.

0.1M Fe^{2+} in the pH range of 3 to 4.5. They found that the sizes of the approximately spherical particles increased from ~1.6 nm to < ~5 nm in diameter within 10 min, and then the particle size stabilized at ~ 5 nm. This particle size is similar to the 2LFh found in our study with TEM. If a similar incipient coalescence process occurs in Fe^{3+} hydrolysis at a pH that metal sorption occurs, metal ions would have access to these smaller particles with larger surface areas (eight times larger geometric surface areas for 1.8 nm diameter spheres than 5 nm diameter spheres), and hence, more sites during CPT experiments, while it is not the case during ADS experiments (Fuller et al., 1993). This may explain the macroscopic observations of markedly different pH sorption edges and isotherms in CPT and ADS experiments, but what happened to the metals sorbed to the initial small particles during coalescence to ~ 5 nm particles is most interesting.

Our high-resolution TEM-AEM (Analytical Electron Microscopy) observations have excluded occlusion of segregated Zn phases (e.g., $Zn(OH)_2$, $ZnCO_3$, ZnO) as a possible coprecipitation mechanism at the time of titration experiments or upon aging for two months to a year, at the ratio of Zn/(Zn+Fe) of 0.05. All known aging effects result in segregation or structural incorporation, but not the reverse (Cornell and Schwertmann, 1996). Thus, it can be postulated that mechanical enveloping, as suggested by previous studies (Schroth, 1994), does not appear to be the mechanism in our experiments. This conclusion is based on evidence from both high-resolution images and analytical electron microscopy, in which no high-concentration Zn^{2+} particles were observed. Images with a point-to-point resolution of 0.17 nm did not detect any surface precipitates of different structures on ferrihydrite particles either. Our conclusions are consistent with published EXAFS results on coprecipitates with similar Zn/(Zn+Fe) ratios (Waychunas et al., 2002, 2003).

The remaining possible mechanisms for Zn^{2+} coprecipitation are the formation of a defective solid solution, or surface adsorption, or a hybrid of both, which are all consistent with the TEM-AEM results within its resolution limits. Geochemical modeling shows that both solid solution models and surface complexation models would fit experimental sorption edge data, with the surface complexation model requiring somewhat higher site density and complexation constants than commonly used in the literature to model surface adsorption experimental data. These theoretical calculations also demonstrate that solid solution can control the aqueous metal concentrations to a lower level than surface adsorption at circumneutral pH. However, Sposito (1986) has long warned of the inefficacy of using macroscopic methods (e.g., the loss of Zn^{2+} from the aqueous solution) to derive molecular level models for sorption. Therefore, results from geochemical modeling generally cannot differentiate solid solution from surface adsorption models.

Zinc can occur in 4, 5, 6, and 7-coordinated geometry in stable compounds, even within a single phase (Wells, 1984). Earlier work by Gerth (1990) shows a linear relationship in goethite cell dimensions as the Zn/(Zn+Fe) ratio in goethite increases and suggests the presence of distorted Zn octahedra in the solid solution. Manceau et al. (2000) interpreted their EXAFS data on trace Zn in natural and synthetic goethite as octahedrally coordinated Zn substituting for Fe, as in a solid solution. In a comprehensive study using EXAFS, Waychunas et al. (2002, 2003) showed spectroscopic evidence against solid solution as the predominant mechanism for coprecipitation in their coprecipitated Zn-ferrihydrite samples unless the solid solutions are highly defective. Our lattice images at 0.17 nm point-to-point resolution did not detect massive defects, and thereby lend support to Waychunas et al.'s spectroscopic arguments. Waychunas et al. (2002, 2003) further found that Zn^{2+} in CPT experiments is bound to ferrihydrite surface as tetrahedral polydentate surface complexes at low-sorption density, while Zn^{2+} in ADS experiments are bound as bidentate inner sphere complexes. Thus, our TEM observations are consistent with the EXAFS and XANES results.

In general, these two sorption mechanisms—solid solution and surface adsorption—should not be mutually exclusive in coprecipitation experiments. The markedly different sorption edges for CPT and ADS experiments essentially call for a somewhat different mechanism for interpreting the CPT experiments from that for ADS experiments. At a Zn/(Zn+Fe) ratio similar to our TEM sample (0.05), Waychunas et al. (2003) found that the average coordination number is 4.4. An algebraic calculation shows this could result from 20% octahedral and 80% tetrahedral coordination of Zn. A 20% of total sorbed Zn as structural incorporation only amounts to 1% Zn for Fe structural substitution. Such distinguishing is, however, within EXAFS analytical uncertainty. On the other hand, even if a solid solution is formed to a small extent, the particle sizes are still small (i.e., ~5 nm diameters; see Figures 4 and 5), and a large percentage of unit cells are exposed at particle surfaces. The large surface areas of these nanoparticles result in a large capacity for surface adsorption. Thus, a combined solid solution and surface adsorption model would only fit the coprecipitation data better, and would satisfy smaller site density and complexation constants in the surface adsorption model. However, without further surface spectroscopic studies, the details cannot be elaborated.

There are many questions that remain unanswered by this study of the Zn^{2+}-Fe^{3+} coprecipitation systems. Different Zn/(Zn+Fe) ratios, different background electrolytes and ionic strength, reaction time between precipitates and Zn^{2+}, filter sizes, sample preservation methods, and aging may all influence the results in this thermodynamically metastable system. A systematic variation of all these parameters is beyond the scope of this study, but would help resolve long-term controversies such as hysteresis in sorption experiments (Ainsworth et al., 1994). We hope the present communication will stimulate more definitive experimental studies on the iron oxyhydroxide/metal coprecipitation systems, which have received much less attention than surface adsorption process.

Acknowledgments—The interest of this research arose from CZ's work on acid mine drainage, in which he observed that highly concentrated iron and toxic metals in low-pH drainage precipitated simultaneously when reacting with calcite-bearing sandstones. This research was accomplished over a long stretch of time. We thank Greg M. Anderson for his encouragement and discussion at the early stage of the work, Dimitri A. Sverjensky and Carla Koretsky for their comments and suggestions on the manuscript. Baolin Deng kindly conducted dupli-

cate experiments (the second set of experiment data) as a verification. Comments from Eric Oelkers, Glen Waychunas, and three anonymous reviewers have greatly helped to improve the quality and presentation of the manuscript.

Associate editor: E. Oelkers

REFERENCES

Ainsworth C. C., Pilon J. L., Gassman P. L., and Van Der Sluys W. G. (1994) Cobalt, cadmium and lead sorption to hydrous iron oxides: residence time effect. *Soil Sci. Soc. Am.* **58,** 1615–1623.

Amonette J. E. and Rai D. (1990) Identification of noncrystalline $(Fe,Cr)(OH)_3$ by infrared spectroscopy. *Clay and Clay Minerals* **38,** 129–136.

Ball J. W. and Nordstrom D. K. (1991) User's manual for WATEQ4F, with revised thermodynamic data base and test cases for calculating speciation of major, trace, and redox elements in natural waters. U.S. Geological Survey Open File Report 91–183.

Bruno J., De Pablo J., Duro L., and Figuerrola E. (1995) Experimental study and modeling of the U(VI)-$Fe(OH)_3$ surface precipitation/coprecipitation equilibria. *Geochim. Cosmochim. Acta* **59,** 4113–4123.

Christl I. and Kretzschmar R. (1999) Competitive sorption of copper and lead at the oxide-water interface: implications for surface site density. *Geochim. Cosmochim. Acta* **63,** 2929–2938.

Cornell R. M. and Schwertmann U. (1996) *The Iron Oxides: Structures, Properties, Reactions, Occurrence and Uses*. VCH, Inc..

Crawford R. J., Harding I. H., and Mainwaring D. E. (1993) Adsorption and coprecipitation of single heavy metal ions onto the hydrated oxides of iron and chromium. *Langmuir* **9,** 3035–3056.

Davis J. A. and Kent D. B. (1990) Surface complexation models in aqueous geochemistry. In *Mineral-water Interface Geochemistry*, Vol. 23 (ed. M. F. and Hochella A. F. White), pp. 177–260, Mineralogical Society of America.

Duff M. C., Coughlin J. U., and Hunter D. B., (2002) Uranium co-precipitation with iron oxide minerals. *Geochim. Cosmochim. Acta* **66,** 3533–3547.

Dzombak D. A. and Morel F. M. M. (1990) *Surface Complexation Modeling: Hydrous Ferric Oxide*. John Wiley & Sons.

Farley K. J., Dzombak D. A., and Morel F. M. M. (1985) Surface precipitation model for the sorption of cations on metal oxides. *J. of Colloid and Interface Science* **106,** 226–242.

Fuller C. C., David J. A., and Waychunas G. A. (1993) Surface chemistry of ferrihydrite: part 2. Kinetics of arsenate adsorption and coprecipitation *Geochim. Cosmochim. Acta* **57,** 2271–2282.

Ganguly J. and Saxena S. K. (1987) *Mixtures and Mineral Reactions*. Springer-Verlag.

Gerth J. (1990) Unit-cell dimensions of pure and trace metal-associated goethite. *Geochim. Cosmochim. Acta* **54,** 363–371.

Janney D. E., Cowley J. M., and Buseck P. R. (2000a) Structure of synthetic 2-line ferrihydrite by electron nanodiffraction. *American Mineralogist* **85,** 1180–1187.

Janney D. E., Cowley J. M., and Buseck P. R. (2000b) Transmission electron microscopy of synthetic 2- and 6-line ferrihydrite. *Clays and Clay Minerals* **48,** 111–119.

Jenne E. A. (1968) Controls on Mn, CO, Ni, Cu, and Zn concentrations in soils and water: the significant role of hydrous Mn and Fe oxides. In *Trace Inorganics in Water* (ed. R. A. Baker), pp. 337–387, American Chemical Society.

Karthikeyan K. G. and Elloitt H. A. (1999) Surface complexation modeling of copper sorption by hydrous oxides of iron and aluminum. *J. of Colloid and Interface Science* **220,** 88–95.

Karthikeyan K. G., Elliott H. A., and Cannon F. S. (1997) Adsorption and coprecipitation of copper with the hydrous oxides of iron and aluminum. *Environ. Sci. Technol.* **31,** 2721–2725.

Karthikeyan K. G., Elloitt H. A., and Chorover J. (1999) Role of surface precipitation in copper sorption by the hydrous oxides of iron and aluminum. *J. of Colloid and Interface Science* **209,** 72–78.

Koretsky C. (2000) The significance of surface complexation reactions in hydrologic systems: a geochemist's perspective. *J. of Hydrology* **230,** 127–171.

Krauskopf K. B. (1956) Factors controlling the concentration of thirteen rare metals in seawater. *Geochim. Cosmochim. Acta* **9,** 1–24.

Manceau A., Charlet L., Boisset M. C., Didier B., and Spadin L. (1992) Sorption and speciation of heavy metals on hydrous Fe and Mn oxides. From microscopic to macroscopic. *Applied Clay Science* **7,** 201–223.

Manceau A., Schlegel M. L., Musso M., Sole V. A., Gauthier C., Petit P. E., and Trolard F. (2000) Crystal chemistry of trace elements in natural and synthetic goethite. *Geochim. Cosmochim. Acta* **64,** 3643–3661.

Martinez C. E. and McBride M. B. (1998) Solubility of Cd^{2+}, Cu^{2+}, Pb^{2+} and Zn^{2+} in aged coprecipitates with amorphous iron hydroxides. *Environ. Sci. Technol.* **31,** 743–748.

Nordstrom D. K., Plummer L. N., Langmuir D., Busenberg E., May H. M., Jones B., and Parkhurst D. L. (1990) Revised chemical equilibrium data for major water-mineral reactions and their limitations. In *Chemical Modeling of Aqueous Systems II* (ed. D. C. Melchior and R. L. Bassett), pp. 398–413, American Chemical Society.

Parkhurst D. L. and Appello A. A. J. (1999) *User's Guide to PHREEQC (Version 2)—A Computer Program for Speciation, Batch-Reaction, One-Dimensional Transport and Inverse Geochemical Modeling.* U.S. Geological Survey, Water Resource Investigation Report 99-4259.

Sass B. M. and Rai D. (1987) Solubility of amorphous chromium (III)-iron (III) hydroxide solid solutions. *Inorganic Chemistry* **26,** 2228–2232.

Schroth J. (1994) Unipure technology removes heavy-metals from waste-water. *Hazardous Waste Consultant* **12,** A33–34.

Schultz M. F., Benjamin M. M., and Ferguson J. F. (1987) Adsorption and desorption of metals on ferrihydrite: reversibility of the reaction and sorption properties of the regenerated solid. *Environmental Science and Technology* **21,** 863–869.

Schulze D. G. and Schwertmann U. (1984) The influence of aluminum on iron oxide: X. Properties of Al-substituted goethites. *Clay Minerals* **19,** 521–539.

Schwertmann U. and Cornell R. M. (1991) *Iron Oxides in the Laboratory: Preparation and Characterization.* VCH.

Schwertmann U., Gasser U., and Sticher H. (1989) Chromium-for-iron substitution in synthetic goethites. *Geochim. Cosmochim. Acta* **53,** 1293–1297.

Shaw S., Benning L. G., Terrill N. J., and Davidson L. (2004) Nucleation and growth of iron oxyhydroxide nanoparticles from solution: An in situ time-resolved small angle X-ray scattering (SAXS) study. *Geochim. Cosmochim. Acta* **68,** A158.

Sposito G. (1984) *The Surface Chemistry of Soils*. Oxford University Press.

Sposito G. (1986) Distinguishing adsorption from surface precipitation. In *Geochemical Processes at Mineral Surfaces,* ACS Symposium Series, (ed. J. A. and Davis K. F. Hayes), pp. 217–228, American Chemical Society.

Stiers W. and Schwertmann U. (1985) Evidence for manganese substitution in synthetic goethite. *Geochim. Cosmochim. Acta* **49,** 909–1911.

Sverjensky D. A. (2003) Standard states for the activities of mineral surface sites and species. *Geochim. Cosmochim. Acta* **67,** 17–28.

Towle S. N., Bargars J. R., Brown G. E., Jr., and Parks G. A. (1997) Surface precipitation of Co(II)(aq) on Al2O3. *J. of Colloid and Interface Science* **187,** 62–82.

Trainor T. P., Brown G. E., Jr., and Parks G. A. (2000) Adsorption and precipitation of aqueous Zn(II) on alumina powders. *J. of Colloid and Interface Science* **231,** 359–372.

Venema P., Hiemstra T., and Van Riemsdijk W. H. (1996) Comparison of different site binding models for cation sorption: description of pH dependency, salt dependency, and cation-proton exchange. *J. of Colloid and Interfacial Sciences* **181,** 45–59.

Wagman D. D., Evans W. H., Parker V. B., Schumm R. H., Halow I., Bailey S. M., Churney K. L., and Nuttall R. L. (1982) The NBS tables of chemical thermodynamic properties: selected values for

inorganic and Cl and C2 substances in SI units. *J. of Physical and Chem. Reference Data* **11,** Supplement No. 2.

Waychunas G. A., Rea, B.A., Fuller C. C., and Davis J. A. (1993) Surface chemistry of ferrihydrite: part 1: EXAFS studies of the geometry of coprecipitated and adsorbed arsenate. *Geochim. Cosmochim. Acta* **57,** 2251–2269.

Waychunas G. A., Fuller C. C., and Davis J. A. (2002) Surface complexation and precipitation geometry for aqueous Zn(II) sorption on ferrihydrite I: X-ray absorption extended fine structure spectroscopy analysis. *Geochim. Cosmochim. Acta* **66,** 1119–1137.

Waychunas G. A., Fuller C. C., Davis J. A., and Rehr J. J. (2003) Surface complexation and precipitate geometry for aqueous Zn(II) sorption on ferrihydrite: II. XANS analysis amd simulation. *Geochim. Cosmochim. Acta* **67,** 1031–1043.

Wells A. F. (1984) *Structural Inorganic Chemistry.* Oxford University Press.

Westall J. C. and Hohl H. (1980) A comparison of electrostatic models for the oxide/solution interface. *Adv. Colloid Interface Sci* **12,** 265–294.

Wolska E. and Schwertmann U. (1993) The mechanism of solid solution formation between goethite and diaspore. *Neves Jahrb Mineral Montash* **5**, 213–223.

Zhu C., Anderson G. M., and Burden D. S. (2002) Natural attenuation reactions at a uranium mill tailings site, western USA. *Ground Water* **40,** 5–13.